

# Co-Training an Observer and an Evading Target

André Brandenburger, Folker Hoffmann, Alexander Charlish  
Fraunhofer FKIE

{andre.brandenburger, folker.hoffmann, alexander.charlish}@fkie.fraunhofer.de

**Abstract**—Reinforcement learning (RL) is already widely applied to applications such as robotics, but it is only sparsely used in sensor management. In this paper, we apply the popular Proximal Policy Optimization (PPO) approach to a multi-agent UAV tracking scenario. While recorded data of real scenarios can accurately reflect the real world, the required amount of data is not always available. Simulation data, however, is typically cheap to generate, but the utilized target behavior is often naive and only vaguely represents the real world. In this paper, we utilize multi-agent RL to jointly generate protagonistic and antagonistic policies and overcome the data generation problem, as the policies are generated on-the-fly and adapt continuously. This way, we are able to clearly outperform baseline methods and robustly generate competitive policies. In addition, we investigate explainable artificial intelligence (XAI) by interpreting feature saliency and generating an easy-to-read decision tree as a simplified policy.

## I. INTRODUCTION

Reinforcement learning (RL) [1] offers the promise of learning the behavior of an agent, requiring only the specification of its reward function. RL could therefore lead to a generic way to perform sensor management, in which only the sensing objective needs to be defined by the system designer. The reinforcement learning algorithm then automatically learns a behavior, called the policy, to fulfill this objective. In many applications, the agents could theoretically learn their policies online in the real world, however the poor performance during early stages of training and in novel, unseen situations make such an approach unpractical. Instead, learning the behavior in a simulated environment and afterwards transferring it to the real world is more feasible. To achieve this, the environment must specify the movement of the non-cooperative targets to be tracked. One could use pre-defined, fixed trajectories, which induces the risk of overfitting to those scenarios. Alternatively, it is possible to let the targets move randomly, which is less realistic. In this work, we instead follow the approach of training against a worst-case target, which counteracts the sensor management. This is achieved by training a target policy with inverted rewards parallel to the sensor management. The policies are trained using multi-agent reinforcement learning based on observations of the platform states and target estimates. A schematic overview of the method can be seen in Fig. 1.

We consider a sensor path planning problem, where the trajectory of an unmanned aerial vehicle (UAV) is optimized. The UAV tracks a mobile ground-based target using a range-bearing sensor, which is restricted in its field of view (FOV). Such measurements are typical for a radar. Utilizing path planning to optimize the performance of a sensor is a classical

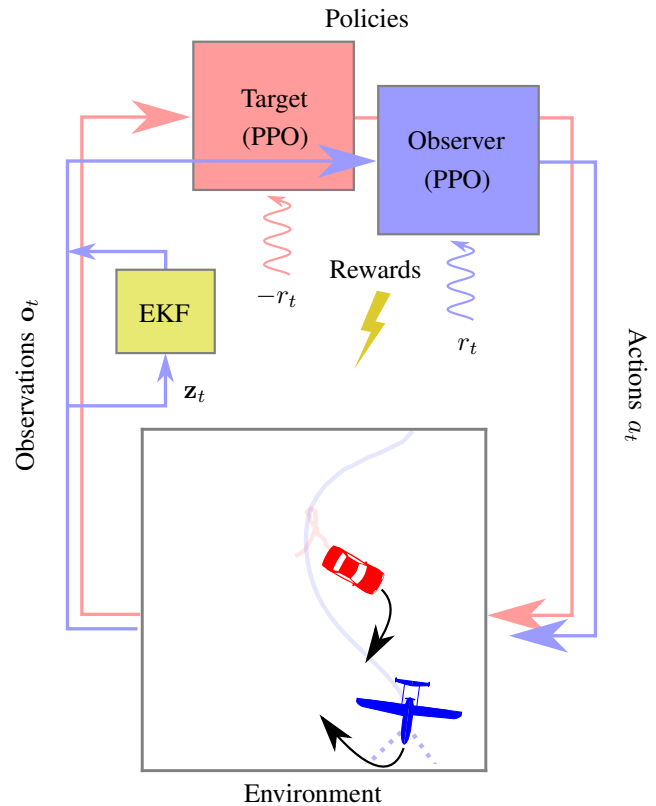


Fig. 1: A schematic overview of our method. We solve a classical UAV control task through reinforcement learning. Two separate policies (top) choose actions (right) based on realistic environment observations (left). An EKF is utilized to filter noisy sensor measurements. Most importantly, we employ contradicting reward signals for the individual policies to innervate antagonistic behaviors.

problem of sensor management and several algorithms have been proposed, mostly based on online trajectory optimization. A common way to evaluate and demonstrate these methods is based on pre-defined target trajectories. For example, [2] optimizes the trajectories of bearing-only sensors and [3] optimizes the trajectories of heterogeneous sensor platforms containing range and/or bearing sensors. In both cases, results are shown for linearly moving targets.

Evaluating a sensor path planning algorithm on a pre-defined scenario is reasonable if the algorithm is guaranteed to also work for other situations. However, when using a

reinforcement learning algorithm, this imposes the risk that the agent behavior overfits to this single scenario. Consequently, the policy would only perform well on the given scenario. Therefore, existing works in path planning using reinforcement learning, have modeled the target behavior as random. The work in [4] optimizes the path of a range-only or bearing-only sensor and models the targets as either stationary or following a 2-D Brownian motion model. The work in [5] considers a target in an urban context, which moves randomly on a partially occluded road grid. The observer learns a behavior to always keep the target in its field of view. In [6], the authors train a policy to localize stationary targets, which are placed randomly based on a prior. We note that some of the works based on online optimization also evaluate their policies using random target behavior [7]. Commonly, this random behavior does not follow a specific intent of the target, but instead is based on a fixed probability distribution on the action space.

However, the assumption that a target moves randomly without intent is often not met in practice. The targets typically have some intent in their behavior. An alternative to the random model would be to find real data based on targets behavior, on which a policy is trained. This would require a large amount of data to avoid overfitting on specific trajectories. In addition, targets might behave differently when the observer policy changes. Lastly, real-world data is mostly difficult and costly to acquire.

Alternatively, a game-theoretic approach can be taken. Instead of modeling specific target trajectories, we assume that the target has the intent to maximally degrade the tracking performance. When training an observer policy under this worst-case assumption, we can expect to achieve better tracking performance for other target behaviors. Such a worst-case target is known as an evading target and has been considered at several places in the literature for path planning based on online optimization. The work in [8] includes, among others, an evasive target model. The target knows the position of the tracking UAVs and always moves away from the closest observer. A more elaborate avoidance model is used in [9], where the ground-based target optimizes its trajectory to hide from an observer between obstacles. The observer takes this target behavior into account when optimizing its own trajectory.

Still, optimizing with respect to a hard-coded evasive target model can lead to overfitting. In this work, we therefore take the approach of training the policy of the evading target in parallel to the policy of the tracking UAV. The target is another agent, whose goal is to deteriorate the tracking performance of the observer as far as possible. If the observer policy specializes too much on the current policy of the target, the target could ideally learn that a change in its behavior leads to the observer tracking it less accurately and, consequently, choose another behavior.

Extending the field of RL to multiple agents is called multi-agent reinforcement learning. In this setting, the policy learned by each agent not only depends on the environment, but also on the learned policies of the other agents. As the other agents

might have different goals, the policy of each agent needs to take the policies of the other agents into account. When these other agents improve in a competitive setting, this leads to a successively increasing difficulty for an agent to achieve its own goals. This feedback can be interpreted as a form of curriculum learning [10]. Co-training of an agent and its antagonist has led to several noteworthy breakthroughs in recent years, especially in the form of self-play, where the policy plays against a potentially different version of itself. Exemplary applications are to learn Go [11] or Starcraft [12].

In this paper, we formulate a setting related to pursuit-evasion problems. In these tasks, a single pursuer or a group needs to catch one or multiple evading targets by reaching their position. Several solutions to this problem are based on explicitly modeling the agent-behavior [13]–[15]. Recently, learning based solutions have been investigated [16], [17]. Training an additional policy for the evading targets can lead to a complex co-evolution of strategies [18]. While addressing a similar application, the problem studied in this paper varies from the pursuit-evasion category mentioned in previous work. In the traditional pursuit-evasion setting, pursuers are required to reach the position of the target. In contrary, this paper addresses a sensor management problem, where a pursuer needs to achieve optimal measurement geometry towards the evading target. The goal is not to reach the target position, but instead to optimally localize it.

In this paper, we do not consider the actual transfer from the simulation to a real system. This adds additional complexities next to the behavior of the target, as the sensor model and the movement model of all platforms must correspond to the real system. Such a sim-to-real transfer is actively researched in the reinforcement learning and robotics communities, using techniques like domain randomization with promising results [19], [20].

In this paper, we apply multi-agent reinforcement learning to the problem of tracking an evading target. In Section II we describe the tracking approach, the sensor management problem and the training method. In Section III we show simulative results and explanations for the trained policies. Finally, Section IV concludes the paper.

## II. METHOD

### A. Multi-Agent Reinforcement Learning

Due to its direct relationship to the trained agent behavior, the simulation environment has to be carefully designed and parameterized. In reinforcement learning, the environment is commonly modelled as a Markov decision process (MDP) and can be described as a tuple  $(S, A, P, R, \gamma)$ . More precisely, it consists of the environment state  $S$ , action space  $A$ , state transition probabilities  $P : S \times A \times S \rightarrow [0, 1]$ , reward function  $R : S \times A \rightarrow \mathbb{R}$  and discount factor  $\gamma \in [0, 1]$ . Typically, agents cannot observe the environment state directly, but only through a projection  $\Omega : S \rightarrow O$  for an observation space  $O$ . Altogether, this yields a Partially Observable Markov Decision Process (POMDP), defined as  $(S, A, P, R, \gamma, O, \Omega)$ .

This environment can be seen as an interaction framework for an agent that seeks to maximize accumulated rewards (or *return*) by choosing propitious actions  $a_t \in A$  from an action space  $A$ . More specifically, this manifests in a mapping  $\Pi : O \rightarrow A$ , called the *policy*. The policy is trained while accounting for all discounted future rewards, enabling the agent to learn long-term behaviors. Traditionally, only a single agent is taken into account. In our application, we consider a multi-agent environment, where two agents, the observer  $\mathcal{O}$  and the target  $\mathcal{T}$  can interact with each other. Consequently, we will define two different sets of observations  $O_{\mathcal{O}}, O_{\mathcal{T}}$ , actions  $A_{\mathcal{O}}, A_{\mathcal{T}}$  and rewards  $R_{\mathcal{O}}, R_{\mathcal{T}}$  for the respective agents.

For more detailed information on modelling RL environments, refer to [1].

### B. Tracking Framework

In this paper, we address the task of trajectory planning for two unmanned platforms. We model one unmanned aerial vehicle (UAV) and one ground-based vehicle. For the sake of simplicity, we consider the task only in two dimensions and neglect the altitude of the platforms. The corresponding states of the agents  $\mathcal{A} \in \{\mathcal{O}, \mathcal{T}\}$  are parameterized by their position  $\mathbf{x}_{\mathcal{A},t} \in \mathbb{R}^2$ , rotation  $\phi_{\mathcal{A},t} \in [-\pi, \pi]$ , forward speed  $v_{\mathcal{A},t} \in \mathbb{R}$  and rotational speed  $\omega_{\mathcal{A},t} \in \mathbb{R}$ . To reduce the complexity of the optimization, we assume  $v_{\mathcal{A},t}$  to be constant, whereas  $\omega_{\mathcal{A},t}$  can be used to steer the vehicle. The simulation frequency is defined as  $\tau > 0$ , meaning at each step  $1/\tau$  seconds elapse. At every time-step  $t \mapsto t + 1$ , the platform state is updated according to classical mechanics

$$\mathbf{x}_{\mathcal{A},t+1} = \mathbf{x}_{\mathcal{A},t} + \frac{1}{\tau} \begin{pmatrix} \cos(\phi_{\mathcal{A},t}) \\ -\sin(\phi_{\mathcal{A},t}) \end{pmatrix} v_{\mathcal{A},t} \quad (1)$$

$$\phi_{\mathcal{A},t+1} = \phi_{\mathcal{A},t} + \frac{1}{\tau} \omega_{\mathcal{A},t}. \quad (2)$$

To model the observer  $\mathcal{O}$  that senses the target platform  $\mathcal{T}$ , we simulate a radar sensor on the observer platform. This radar yields noisy local measurements  $\mathbf{z}_{\mathcal{T},t}$  of the target relative to the observer in polar coordinates, such that

$$\Delta \mathbf{x}_t = \mathbf{x}_{\mathcal{O},t} - \mathbf{x}_{\mathcal{T},t} \quad (3)$$

$$d_t = \|\Delta \mathbf{x}_t\|_2 \quad (4)$$

$$\theta_{\mathcal{T},t} = \text{atan2}((\Delta \mathbf{x}_t)_y, (\Delta \mathbf{x}_t)_x) - \phi_{\mathcal{O},t} \quad (5)$$

$$\mathbf{z}_{\mathcal{T},t} \sim \mathcal{N}([d_t, \theta_{\mathcal{T},t}]; \text{diag}(\sigma_d^2, \sigma_\theta^2)). \quad (6)$$

The front-facing sensor is restricted to a fixed FOV with constant opening  $0 < \alpha \leq 2\pi$ , where a measurement is only registered iff  $|\theta_{\mathcal{T},t}| < \frac{1}{2}\alpha$ . Additionally, we define the number of time steps since the last registered measurement as  $\Delta t_{t,z}$ .

We employ an extended Kalman filter (EKF) to reconstruct a target estimate from the noisy sensor measurements. The EKF utilizes the true sensor noise matrix and the popular piecewise constant white acceleration dynamics model [21]. This results in the target track  $([\tilde{\mathbf{x}}_{\mathcal{T},t}, \tilde{\mathbf{v}}_{\mathcal{T},t}], \mathbf{P}_{\mathcal{T},t})$ , which is an estimate of the target position and velocity with corresponding covariance  $\mathbf{P}_{\mathcal{T},t}$  in the global frame.

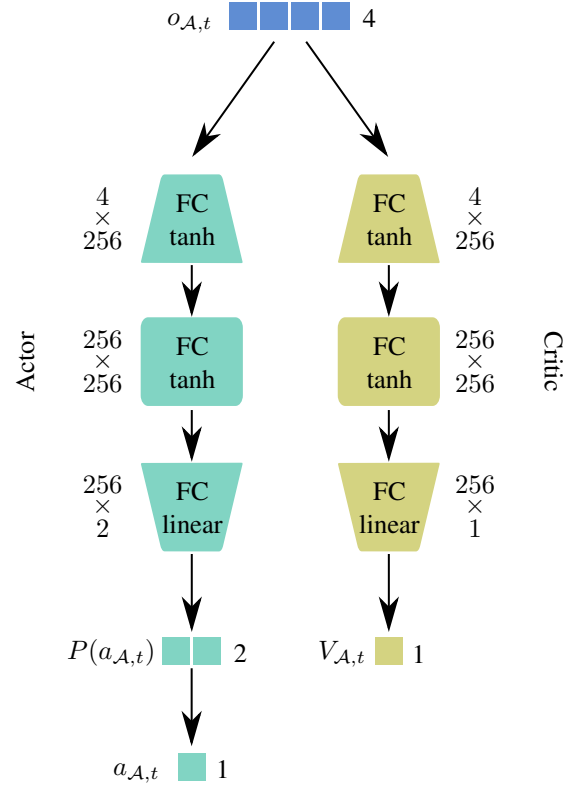


Fig. 2: The model architecture for the learned policies. On the left, the actor network is shown, which learns the parameterization of a gaussian action distribution. On the right we display the critic network. The models utilize fully connected (FC) layers with *tanh* activation for the hidden units and linear activation for the output units.

Similar to  $d_t$  and  $\theta_{\mathcal{T},t}$ , we define

$$\Delta \tilde{\mathbf{x}}_t = \mathbf{x}_{\mathcal{O},t} - \tilde{\mathbf{x}}_{\mathcal{T},t} \quad (7)$$

$$\tilde{d}_t = \|\Delta \tilde{\mathbf{x}}_t\|_2 \quad (8)$$

$$\tilde{\theta}_{\mathcal{T},t} = \text{atan2}((\Delta \tilde{\mathbf{x}}_t)_y, (\Delta \tilde{\mathbf{x}}_t)_x) - \phi_{\mathcal{O},t}, \quad (9)$$

based on the constructed track.

### C. Agent Models

For our method, we utilize the Proximal Policy Optimization (PPO) algorithm [22], which has proven as highly performant in a wide range of tasks such as UAV control [6], [23]. A schematic of the network architecture is shown in Fig. 2. As seen before, the use of RL methods requires the careful definition of the observation- and action space, as well as a reward function that reflects the goal of the optimization.

1) *Observation Spaces*: To enable us to supply the agents with a scalar indicator of uncertainty instead of the multi-dimensional covariance, we calculate the entropy

$$S_t = \frac{1}{2} \ln \det(2\pi e \mathbf{P}_{\mathcal{T},t}). \quad (10)$$

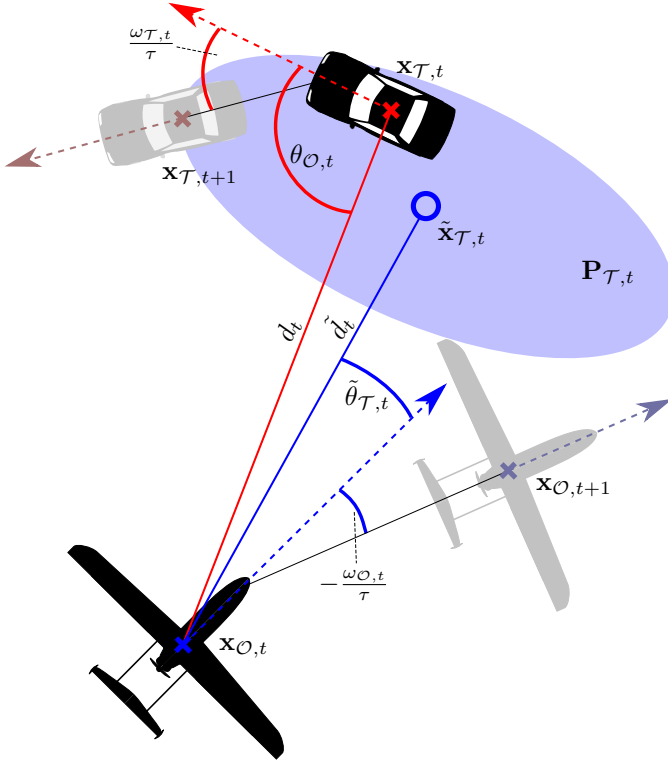


Fig. 3: A partial visualization of the observation space. The UAV (bottom left) builds an estimate  $\tilde{\mathbf{x}}_{\mathcal{T},t}$  of the target (top center) with corresponding covariance  $\mathbf{P}_{\mathcal{T},t}$ . This estimate is transformed into local polar coordinates  $(\tilde{d}_t, \tilde{\theta}_{\mathcal{T},t})$  before it is added to the observation vector. Similarly, the target observation uses a polar coordinate representation of the true UAV position. Both platforms change heading with respect to their rotational velocities  $\omega_{\mathcal{O},t}$  and  $\omega_{\mathcal{T},t}$ .

In addition, we process the time since the last measurement  $\Delta t_{t,z}$  using a decay function

$$\kappa_t = k^{-\Delta t_{t,z}}, \quad (11)$$

for a  $k > 1$ . In contrast to  $\Delta t_{t,z}$ ,  $\kappa_t$  is bounded, which is beneficial for training stability.

Accordingly, we summarize the environment state by projecting to the agent observation

$$\mathbf{o}_{\mathcal{O},t} = [\omega_{\mathcal{O},t}, \kappa_t, \tilde{d}_t, \sin(\tilde{\theta}_{\mathcal{T},t}), \cos(\tilde{\theta}_{\mathcal{T},t}), S_t] \quad (12)$$

$$\mathbf{o}_{\mathcal{T},t} = [\omega_{\mathcal{T},t}, d_t, \sin(\theta_{\mathcal{O},t}), \cos(\theta_{\mathcal{O},t})], \quad (13)$$

with  $\theta_{\mathcal{O},t}$  defined analogously to  $\theta_{\mathcal{T},t}$ . Both angles are decomposed into sine and cosine terms, correcting the discontinuity of the angle representation at  $\pm\pi$ . A partial illustration of the observation space is shown in Fig. 3.

This way, the observations yield a concise representation of the environment state. For the observer, this not only includes information about the targets position and platform velocity, but also the time-since-measurement decay  $\kappa_t$  and the uncertainty measure  $S_t$ . While  $S_t$  is crucial for assessing the track uncertainty,  $\kappa_t$  provides a notion of time to the

otherwise time-agnostic observer, allowing for more complex behaviors. While the observer is based on the estimated target position, the target is given the true position of the observer. Note that, the goal in this paper is to train an observer policy, which is robust against maneuvering and evading targets. By making the worst case assumption of the target knowing the true position of the observer, the target is strengthened in its role as the antagonist.

Note that, by normalizing the observations  $\mathbf{o}_{\mathcal{A},t}$  with the limits  $d_{\max}$  and  $S_{\max}$ , it is possible to achieve  $\mathbf{o}_{\mathcal{A},t} \in [-1, 1]$ . Since normalized values are typically easier to learn by neural networks, we utilize this augmentation to increase the training performance. The parameter  $d_{\max}$  denotes the maximal range of interest, and  $S_{\max}$  a value empirically higher than any encountered track entropy.

2) *Action Spaces*: To enable the agents to navigate in the environment, we accept actions  $a_{\mathcal{A},t} \in [-1, 1]$  that steer the platform, while complying with velocity limits  $\omega_{\mathcal{A},\min}, \omega_{\mathcal{A},\max}$ , such that

$$\omega_{\mathcal{A},t} = \frac{1}{2} (\omega_{\mathcal{A},\max} - \omega_{\mathcal{A},\min}) (a_{\mathcal{A},t} + 1) + \omega_{\mathcal{A},\min}. \quad (14)$$

Thus, both agents are able to adapt their rotational velocities to control their movement in the environment.

3) *Reward Functions*: The reward function captures the optimization goals of the RL agents. Since we consider a sensor management task, the observer will maximize the tracking performance, which we formulate as minimization of the track entropy  $S_t$ . On the contrary, the target will attempt to counteract the observer as well as possible. Consequently, we define the rewards as

$$r_{\mathcal{O},t} = 1 - \frac{S_t}{S_{\max}} \quad (15)$$

$$r_{\mathcal{T},t} = -r_{\mathcal{O},t}. \quad (16)$$

This way, we set conflicting objectives for the observer  $\mathcal{O}$  and the target  $\mathcal{T}$ , since the observer will try to increase the track accuracy, whereas the target aims to reduce it.

4) *Termination Criteria*: A single simulation run is ended if any of the following termination criteria

$$t > t_{\max} \quad d_t > d_{\max} \quad \tilde{d}_t > d_{\max}, \quad (17)$$

is fulfilled, with a maximum run length  $t_{\max}$  and maximum target distance  $d_{\max}$ . As common in the reinforcement learning literature, we denote such a single simulation run as an episode. These termination criteria contribute to richer training data, as uninteresting situations are not recorded. This mainly comes into effect during early stages of training, where the policies have not yet captured their respective goals. Recognize, that negative rewards give an incentive to terminate, whereas positive rewards encourage the continuation of episodes. Therefore, we ensure that  $r_{\mathcal{O},t} > 0$  and  $r_{\mathcal{T},t} < 0$  hold. This causes the observer to prefer long episodes, whereas the target is inclined to end the episode, if possible.

### III. EXPERIMENTAL RESULTS

Firstly, we define simple baseline methods, which are used as a comparison for the performance of our approach. As a naive agent, a random policy is constructed, where actions  $a_t \in [-1, 1]$  are drawn uniformly at random:

$$a_{\mathcal{O}_R,t} \sim U(-1, 1) \quad (18)$$

$$a_{\mathcal{T}_R,t} \sim U(-1, 1) \quad (19)$$

Secondly, we define proportional control policies (P-Controller), which based on the angular deviations  $\theta_{\mathcal{A},t}$  and gains  $K_{\mathcal{A}}$ , steer the observer towards the target and the target away from the observer:

$$a_{\mathcal{O}_P,t} = K_{\mathcal{O}} \frac{\theta_{\mathcal{T},t}}{\pi} \quad (20)$$

$$a_{\mathcal{T}_P,t} = \text{sgn}(\theta_{\mathcal{O},t}) K_{\mathcal{T}} \left( 1 - \frac{|\theta_{\mathcal{O},t}|}{\pi} \right) \quad (21)$$

This way, we achieve simple baseline behaviors for evasion and tracking. Note that, those policies are based on the ground truth direction towards the target. This makes the baseline stronger and assures that it does not fail in situations, where the track is inaccurate.

Furthermore, in the course of this evaluation, we use the following environment parameterization:

|   |  |                                      |
|---|--|--------------------------------------|
| $\alpha = 1.4 \text{ rad}$                      | $\sigma_d = 40 \text{ m}$                      | $\sigma_\theta = 0.005 \text{ rad}$  |
| $k = 1.05$                                      | $S_{\max} = 50$                                | $d_{\max} = 5000 \text{ m}$          |
| $t_{\max} = 20 \text{ min}$                     | $\tau = 0.5 \text{ Hz}$                        | $\gamma = 0.99$                      |
| $\omega_{\mathcal{O},\min} = -0.25 \text{ rad}$ | $\omega_{\mathcal{O},\max} = 0.25 \text{ rad}$ | $v_{\mathcal{O},x} = 50 \text{ m/s}$ |
| $\omega_{\mathcal{T},\min} = -0.75 \text{ rad}$ | $\omega_{\mathcal{T},\max} = 0.75 \text{ rad}$ | $v_{\mathcal{T},x} = 20 \text{ m/s}$ |
| $K_{\mathcal{O}} = 1.0$                         | $K_{\mathcal{T}} = 0.2$                        |                                      |

#### A. Performance

We train the model on a standard work station machine, with a *AMD Ryzen 7 PRO 3700U*, utilizing 3 CPUs and no GPU. It is expected that inference should also be possible on a smaller, embedded system. In total, the training over 0.8M environment interactions takes approximately 45 minutes. Our implementation is based on *Ray RLLib* [24] with a TensorFlow backend, which allows for high scalability if needed, reducing the training time even further.

To validate network convergence, we have performed 50 training runs with approximately 1.5M environment steps. The resulting observer returns during training are shown in Fig. 4. Note that, the mean observer performance only marginally increases after 0.8M steps, indicating that the policy has converged. As seen in Fig 4, our model not only outperforms the random agent, but also consistently exceeds the performance of the P-Controller for all trained policies. It can be seen that, since the target policy is trained in conjunction with the observer, the difficulty of the task increases over time. This is clearly reflected in the P-Controller performance, which decreases over the course of the training.

In Tables I and II we compare the performance and stability of the baseline methods to our trained agents at 0.8M steps. As

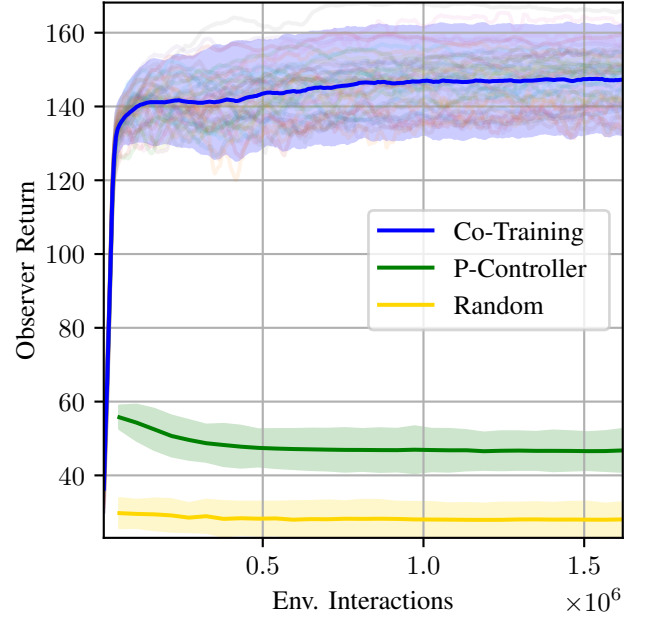


Fig. 4: Observer learning curves. The returns of the individual training runs for the proposed approach are shown as the shaded lines and the mean performance as the opaque blue line. The opaque green line shows the mean performance of the P-Controller observer, whereas the random policy is displayed in yellow. The shaded regions correspond to  $\mu \pm 2\sigma$ .

already shown in Fig. 4, our approach clearly outperforms the simpler baseline solutions. Observe in Table I, however, that the best agent against a random observer is the P-Controller target. As the best strategy against an incapable observer is to simply maximize the distance to the observer and end the episode, the P-Controller performs better in that scenario. This shows that our approach implicitly assumes a capable opponent policy. Nevertheless, this is a valid assumption for most real world applications. Furthermore, we show low mean performance variance for fixed policies in Table II.

In addition, we assess the mean optimal subpattern assignment (OSPA) metric [25] over the different models. This metric combines information on the track accuracy with the number of correctly tracked targets. We compute the average OSPA metric over episodes with a fixed duration  $t_{\max}$ . According to Eq. 17, a single episode terminates at time  $t_{\text{term}} < t_{\max}$  if the target can be considered lost by the observer. Thus, if an episode terminates early, we view the target track as dropped for the remaining episode. This allows us to reformulate the OSPA metric for a single target as

$$\frac{1}{t_{\max}\tau} \left( \sum_t^{t_{\text{term}}} [\min(\|\mathbf{x}_{\mathcal{T},t} - \tilde{\mathbf{x}}_{\mathcal{T},t}\|_2, c)] + (t_{\max} - t_{\text{term}})\tau c \right), \quad (22)$$

with a cutoff distance  $c$ . In contrast to the return, the OSPA metric is a direct indicator of the tracking performance. Anal-

| Target \ Observer | Co-Training       | P-controller     | Random          |
|-------------------|-------------------|------------------|-----------------|
| Co-Training       | 146.34 $\pm$ 15.1 | 46.90 $\pm$ 5.6  | 28.21 $\pm$ 5.1 |
| P-controller      | 153.79 $\pm$ 39.6 | 130.93 $\pm$ 0.0 | 22.29 $\pm$ 0.0 |
| Random            | 151.74 $\pm$ 21.6 | 54.44 $\pm$ 0.0  | 28.51 $\pm$ 0.0 |

TABLE I: Mean observer episode return  $\mu \pm 2\sigma$  compared to baseline methods after 0.8M training steps. The standard deviation  $\pm 2\sigma$  indicates the mean performance variation after re-training the model from scratch. Note that, the first row corresponds to the results of Fig. 4. Since the standard deviation is calculated over the different training runs,  $\sigma = 0$  holds when comparing the static baseline methods

| Target \ Observer | Co-Training | P-controller | Random     |
|-------------------|-------------|--------------|------------|
| Co-Training       | $\pm 10.7$  | $\pm 10.4$   | $\pm 37.0$ |
| P-controller      | $\pm 11.9$  | $\pm 5.6$    | $\pm 29.8$ |
| Random            | $\pm 6.6$   | $\pm 18.7$   | $\pm 37.9$ |

TABLE II: Mean observer episode return standard deviations  $\pm 2\sigma$  after 0.8M training steps. The standard deviation  $\pm 2\sigma$  shows the mean performance deviation of fixed policies over different test episodes. Consequently, the standard deviation indicates how much the return of a single trained policy fluctuates during different inference episodes.

| Target \ Observer | Co-Training  | P-controller | Random       |
|-------------------|--------------|--------------|--------------|
| Co-Training       | 271 $\pm$ 94 | 425 $\pm$ 28 | 471 $\pm$ 25 |
| P-controller      | 158 $\pm$ 93 | 348 $\pm$ 0  | 464 $\pm$ 0  |
| Random            | 194 $\pm$ 50 | 457 $\pm$ 0  | 453 $\pm$ 0  |

TABLE III: Comparison of the mean OSPA metric  $\mu \pm 2\sigma$  after 0.8M training steps with cutoff distance  $c = 500\text{m}$ . The lower the OSPA metric, the better the localization of the target. Since the standard deviation is calculated over the different training runs,  $\sigma = 0$  holds when comparing the static baseline methods.

ogous to previous evaluations, the OSPA metric is computed over 50 training runs after 0.8M steps of training, each of which is evaluated over 50 test episodes. In Table III it can be seen that the Co-Training method also outperforms the baseline approaches with respect to this more general metric.

For further investigation, we use the model with median return at 0.8M steps. This way, we ensure that representative results are achieved without bias towards particularly performant models.

### B. Policy Explanation (XAI)

As more complex artificial intelligence (AI) approaches find their ways into our lives, model explanation strongly gains importance. For instance, the reasoning of neural network models is opaque by nature, which undermines trust for non-experts and makes them hard to employ for security critical systems. There are already numerous suggestions on how to explain AI methods, an overview about many methods can be found in [26]. In this paper, we explain the learned policy on the basis of two approaches: The ad-hoc analysis of the feature importance using saliency and the post-hoc policy approximation using decision trees. Note that, although we

only evaluate the observer policy, the same procedures can be applied to investigate the target policy.

Similar to the neural network training mechanism, it is possible to utilize the gradients to visualize importance of specific input features given a network output. This is particularly popular in computer-vision approaches, where the gradients can be processed to *saliency maps*, which can be used to find important regions of the input image. In our approach, it is possible to utilize the same principle: By plotting  $\frac{da_{O,t}}{do_{O,t}}$ , we can assess the sensitivity of the action  $a_{O,t}$  with respect to the observation  $o_{O,t}$ . A sequence of (non-consecutive) frames with the corresponding gradients is shown in Fig. 5. Note that, the observer succeeds in tracking the target, while regularly maneuvering over it and taking strong turns to keep it in the observers limited FOV. On the other hand, the target apparently follows the observer. Although this might appear to be a counter-intuitive strategy to avoid tracking, this policy allows the target to exploit the limited FOV of the observer. By keeping the distance to the observer small, the target is able to repeatedly find its way behind the observer, becoming invisible for the observer and forcing it to take expensive, strong turns to relocate the target.

In the plotted normalized gradients, it is apparent, that the most important features are  $\kappa_t$ ,  $\tilde{d}_t$  and  $S_t$ , whereas  $\omega_{O,t}$ ,  $\sin(\tilde{\theta}_{\mathcal{T},t})$  and  $\cos(\tilde{\theta}_{\mathcal{T},t})$  are less significant for this episode. Note that, this only explains the policy locally. The observations in the recorded episodes are not uniformly distributed, but depend on the policy. Therefore, an analysis based on those observations is biased towards regions of the state space that are frequently visited by the policy. While this local explanation can give insight in the policy behavior in the mean case, it is often imperative to also assess the behavior in less likely edge cases, which will be part of the next technique.

To enable global understanding of the policy, we construct a post-hoc decision tree model of the observer. By evaluating the agent reactions  $a_{O,t}$  on a uniform 6-D grid of observations  $o_{O,t}$ , it is possible to generate representative samples of the policy  $\Pi : O \rightarrow A$ . In each dimension of the observation, we generate 21 samples. Subsequently, we utilize these samples to train a decision tree regressor, while employing pruning to ensure generalization and to limit the size of the tree. An excerpt of the resulting tree can be seen in Fig. 6, where the color indicates the action that would be taken if the tree is evaluated until the corresponding node. Note that, the observations  $\sin(\tilde{\theta}_{\mathcal{T},t})$ ,  $\cos(\tilde{\theta}_{\mathcal{T},t})$  are considered jointly for the tree generation, as their values are correlated through  $\tilde{\theta}$ . Generally, negative actions are located on the left side of the tree, whereas positive actions tend to be produced by the right most nodes. As common with decision trees, nodes in the upper levels of the tree can be seen as the most important nodes, whereas lower levels only handle details of the task. As expected, the decision tree only partially agrees with the saliency analysis. For uniformly sampled observations, the track angle  $\tilde{\theta}_{\mathcal{T},t}$  and the last action  $\omega_{O,t}$  significantly gain importance, whereas the previously important track distance  $\tilde{d}_t$  does not occur at the top layers.

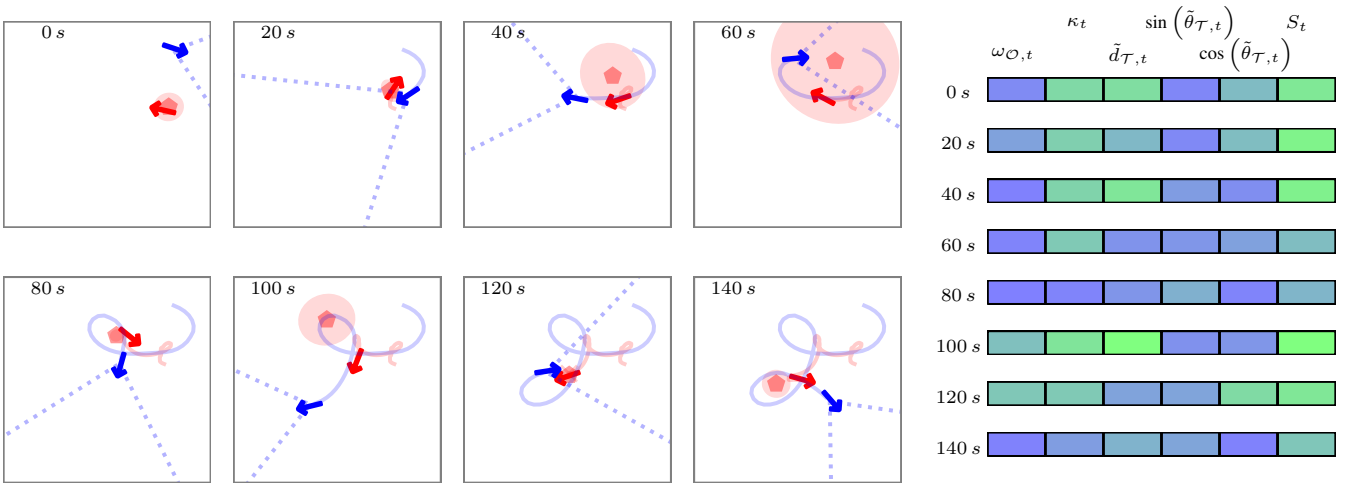


Fig. 5: Behavior of the median policies trained for 0.8M environment interactions (left) and gradients with respect to the agent observations (right). The blue arrow denotes the observer pose, with the field of view as the dashed blue line and the full observer trajectory in shaded blue. Analogously, the target is shown in red, with the target estimate as the red pentagon with corresponding standard deviation  $2\sigma$  shown as the red ellipses. On the right, the normalized gradients  $\frac{da_{O,t}}{d\omega_{O,t}}$  are plotted for each of the time steps, where blue indicates low and green represents high gradients.

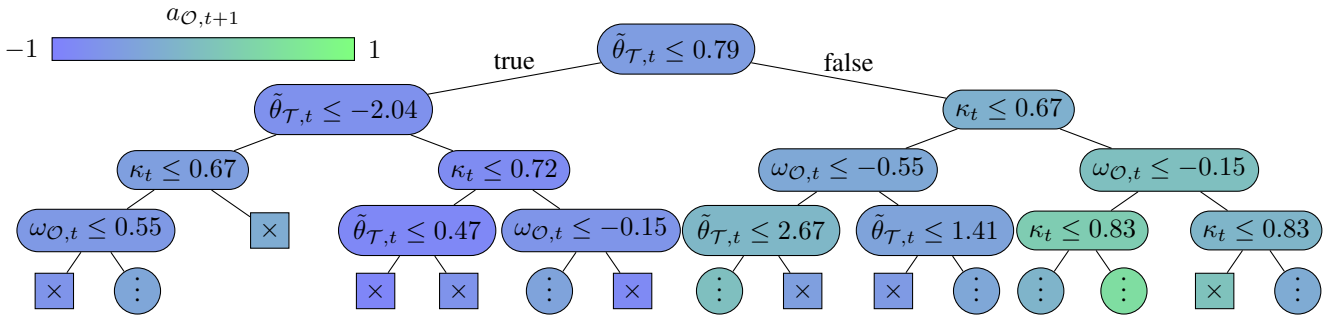


Fig. 6: Decision tree of the median-performance model generated using artificial observations. The nodes resemble a numerical decision criterion, where the color indicates the action that would be taken at that node. By traversing the tree downwards, the chosen actions mimic the trained policy closer. Vertical dots show truncated splitting nodes, whereas leaf nodes are displayed as "x".

In addition, it is possible to analyze individual paths in the tree to understand the general decision process of the policy. For example, the shown tree produces the strongest turns for the following criteria:

$$a_{O,t} \approx -1 : -120^\circ < \tilde{\theta}_{T,t} \leq 27^\circ \wedge \kappa_t \leq 0.72$$

$$a_{O,t} \approx 1 : 45^\circ < \tilde{\theta}_{T,t} \wedge 0.83 < \kappa_t \wedge \omega_{O,t} \leq -0.15$$

In the first case, the agent takes a strong right turn if the target estimate is to its right, but the target has not been seen for at least 8 steps (encoded in  $\kappa_t$ ). This stands in contrast to the second case, where the platform rotated away from the target in the previous step. Now the target is on the left of the platform, slightly outside the observer FOV. As the target was seen at most 3 steps ( $\kappa_t$ ) before, it can be expected that a strong left turn moves the target back into the field of view. Due to the different values of  $\kappa_t$ , the two cases are fundamentally different, since the right turn is induced

by the absence of information, whereas the left turn is taken due to recent measurements. However, it must be noted that the decision tree is not an exact approximation of the true policy, due to the coarse per-dimension sample size, as well as inherently due to a finite tree. Consequently, it can not be expected to capture the full potential of the agent, prohibiting the exhaustive explanation through this method. Still, the decision tree gives important insight into the general decision process of the otherwise opaque neural network model.

#### IV. CONCLUSION

In this paper, we have presented an approach to jointly train observer and target policies in an UAV tracking scenario.

The successful implementation of our method opens the door to numerous areas of research and applications. For instance, the agents can be utilized to generate trajectories, which in turn can be used as training or evaluation data

for other approaches. Traditionally, generating these type of behavioral trajectories often necessitates recording real world data, which can be expensive due to factors such as hardware wear and supervision by human experts. While hand-crafted simulated trajectories can be cheaper, they are still time-consuming to design. With suitable reward functions, these costly methods of data acquisition can now be substituted by trained agents, which can mirror the competitive behavior of typical real-world scenarios. Although finding matching reward functions can be challenging, they are mostly significantly easier to formulate than the policies themselves.

Additionally, and most apparently, our models can be directly used for controlling UAVs in a tracking scenario with an evading target. Previous methods, that were either based on simple behavioral procedures or trained on recorded target trajectories, are prone to overfitting and do not properly reflect real-world cases. By co-training both agents hand-in-hand, we generate the data on-line and thus mitigate these shortcomings.

Moreover, the method promises to perform well on more challenging tasks, which may manifest in higher measurement noise, more mobile targets or occlusion. Investigation and adaption on these scenarios poses an interesting foundation for future work. Furthermore, it is possible to incorporate a specific sensor model for the target. This can lead to different behavior, as the observer may learn to exploit potential blind spot of the target, deteriorating its evasion capabilities

Additional future work could also analyze the policies in more depth, utilizing more sophisticated XAI strategies and exchanging with domain experts. Finally, insights of these explanations can be used to refine the model.

## REFERENCES

- [1] R. S. Sutton and A. G. Barto, *Reinforcement Learning*, 2nd ed. Cambridge, Massachusetts, USA: MIT Press, 2018.
- [2] M. L. Hernandez, "Optimal sensor trajectories in bearings-only tracking," in *The 7th International Conference on Information Fusion (FUSION)*. Stockholm, Sweden: IEEE, 2004, pp. 1–8.
- [3] K. Zhou and S. I. Roumeliotis, "Multirobot active target tracking with combinations of relative observations," *IEEE Transactions on Robotics*, vol. 27, no. 4, pp. 678–695, Aug. 2011.
- [4] S. Engin and V. Isler, "Active localization of multiple targets from noisy relative measurements," in *International Workshop on the Algorithmic Foundations of Robotics (WAFR)*, Oulu, Finland, 2020, pp. 398–413.
- [5] S. Bhagat and P. Sujit, "UAV target tracking in urban environments using deep reinforcement learning," in *2020 International Conference on Unmanned Aircraft Systems (ICUAS)*. Athens, Greece: IEEE, 2020, pp. 694–701.
- [6] F. Hoffmann, A. Charlish, M. Ritchie, and H. Griffiths, "Sensor path planning using reinforcement learning," in *2020 IEEE 23rd International Conference on Information Fusion (FUSION)*, Virtual Conference, 2020, pp. 1–8.
- [7] S. A. Miller, Z. A. Harris, and E. K. Chong, "A POMDP framework for coordinated guidance of autonomous UAVs for multitarget tracking," *EURASIP Journal on Advances in Signal Processing*, vol. 2009, p. 724597, 2009.
- [8] S. Ragi and E. K. P. Chong, "UAV path planning in a dynamic environment via partially observable markov decision process," *IEEE Transactions on Aerospace and Electronic Systems*, vol. 49, no. 4, pp. 2397–2412, 2013.
- [9] P. Theodorakopoulos and S. Lacroix, "UAV target tracking using an adversarial iterative prediction," in *International Conference on Robotics and Automation*. Kobe, Japan: IEEE, 2009, pp. 2866–2871.
- [10] S. Narvekar, B. Peng, M. Leonetti, J. Sinapov, M. E. Taylor, and P. Stone, "Curriculum learning for reinforcement learning domains: A framework and survey," *Journal of Machine Learning Research*, vol. 21, no. 181, pp. 1–50, 2020.
- [11] D. Silver, A. Huang, C. J. Maddison, A. Guez, L. Sifre, G. van den Driessche, J. Schrittwieser, I. Antonoglou, V. Panneershelvam, M. Lanctot, S. Dieleman, D. Grewe, J. Nham, N. Kalchbrenner, I. Sutskever, T. Lillicrap, M. Leach, K. Kavukcuoglu, T. Graepel, and D. Hassabis, "Mastering the game of Go with deep neural networks and tree search," *Nature*, vol. 529, no. 7587, pp. 484–489, Jan. 2016.
- [12] O. Vinyals, I. Babuschkin, W. M. Czarnecki, M. Mathieu, A. Dudzik, J. Chung, D. H. Choi, R. Powell, T. Ewalds, P. Georgiev, J. Oh, D. Horgan, M. Kroiss, I. Danihelka, A. Huang, L. Sifre, T. Cai, J. P. Agapiou, M. Jaderberg, A. S. Vezhnevets, R. Leblond, T. Pohlen, V. Dalibard, D. Budden, Y. Sulsky, J. Molloy, T. L. Paine, C. Gulcehre, Z. Wang, T. Pfaff, Y. Wu, R. Ring, D. Yogatama, D. Wünsch, K. McKinney, O. Smith, T. Schaul, T. Lillicrap, K. Kavukcuoglu, D. Hassabis, C. Apps, and D. Silver, "Grandmaster level in StarCraft II using multi-agent reinforcement learning," *Nature*, vol. 575, no. 7782, pp. 350–354, Nov. 2019.
- [13] M. Janosov, C. Virágh, G. Vásárhelyi, and T. Vicsek, "Group chasing tactics: how to catch a faster prey," *New Journal of Physics*, vol. 19, no. 5, p. 053003, 2017.
- [14] J. Li, M. Li, Y. Li, L. Dou, and Z. Wang, "Coordinated multi-robot target hunting based on extended cooperative game," in *2015 IEEE International Conference on Information and Automation (ICIA)*. Lijiang, China: IEEE, August 2015, pp. 216–221.
- [15] L. Angelani, "Collective predation and escape strategies," *Physical Review Letters*, vol. 109, no. 11, pp. 1–5, 2012.
- [16] C. de Souza, R. Newbury, A. Cosgun, P. Castillo, B. Vidolov, and D. Kulic, "Decentralized multi-agent pursuit using deep reinforcement learning," oct 2020. [Online]. Available: <http://arxiv.org/abs/2010.08193>
- [17] R. Lowe, Y. Wu, A. Tamar, J. Harb, P. Abbeel, and I. Mordatch, "Multi-agent actor-critic for mixed cooperative-competitive environments," in *Advances in Neural Information Processing Systems (NIPS)*, Los Angeles, CA, USA, 2017, pp. 6380–6391.
- [18] B. Baker, I. Kanitscheider, T. Markov, Y. Wu, G. Powell, B. McGrew, and I. Mordatch, "Emergent tool use from multi-agent autocurricula," in *Ninth International Conference on Learning Representations (ICLR)*, Virtual Conference, 2020, pp. 1–28.
- [19] X. B. Peng, M. Andrychowicz, W. Zaremba, and P. Abbeel, "Sim-to-real transfer of robotic control with dynamics randomization," in *2018 IEEE International Conference on Robotics and Automation (ICRA)*. Brisbane, QLD, Australia: IEEE, May 2018, pp. 3803–3810.
- [20] OpenAI, I. Akkaya, M. Andrychowicz, M. Chociej, M. Litwin, B. McGrew, A. Petron, A. Paino, M. Plappert, G. Powell, R. Ribas, J. Schneider, N. Tezak, J. Tworek, P. Welinder, L. Weng, Q. Yuan, W. Zaremba, and L. Zhang, "Solving rubik's cube with a robot hand," 2019. [Online]. Available: <https://arxiv.org/abs/1910.07113>
- [21] Y. Bar-Shalom, X. R. Li, and T. Kirubarajan, *Estimation with applications to tracking and navigation: theory algorithms and software*. John Wiley & Sons, 2004, pp. 273–274.
- [22] J. Schulman, F. Wolski, P. Dhariwal, A. Radford, and O. Klimov, "Proximal policy optimization algorithms," 2017. [Online]. Available: <http://arxiv.org/abs/1707.06347>
- [23] W. Koch, R. Mancuso, R. West, and A. Bestavros, "Reinforcement learning for UAV attitude control," *ACM Transactions on Cyber-Physical Systems*, vol. 3, no. 2, Feb. 2019.
- [24] E. Liang, R. Liaw, R. Nishihara, P. Moritz, R. Fox, K. Goldberg, J. E. Gonzalez, M. I. Jordan, and I. Stoica, "RLlib: Abstractions for distributed reinforcement learning," in *International Conference on Machine Learning (ICML)*, Stockholm, Sweden, 2018.
- [25] D. Schuhmacher, B. T. Vo, and B. N. Vo, "A consistent metric for performance evaluation of multi-object filters," *IEEE Transactions on Signal Processing*, vol. 56, no. 8, pp. 3447–3457, 2008.
- [26] A. Barredo Arrieta, N. Díaz-Rodríguez, J. Del Ser, A. Bennetot, S. Tabik, A. Barbado, S. Garcia, S. Gil-Lopez, D. Molina, R. Benjamins, R. Chatila, and F. Herrera, "Explainable artificial intelligence (XAI): Concepts, taxonomies, opportunities and challenges toward responsible ai," *Information Fusion*, vol. 58, pp. 82–115, 2020.